

Linear shear flow past a hemispherical droplet adhering to a solid surface

K. Sugiyama¹ and M. Sbragaglia¹

¹*Faculty of Applied Sciences, IMPACT, and Burgerscentrum,
University of Twente, P.O. Box 217, AE 7500 Enschede, The Netherlands*

In this paper we investigate the properties of a three dimensional Stokes problem when a hemispherical droplet is introduced into a linear shear flow past a flat plane. The exact solution is computed as a function of the viscosity ratio between the droplet and the fluid and generalizes the solution for the hemispherical no-slip bump given in an earlier paper by Price [7], here recovered in the limiting case of highly viscous droplet. Several expressions including the torque and the force acting on the drop will be considered as well as the role of the deformations on the surface for finite Capillary numbers.

PACS numbers: 47.10.-g, 47.15.-x, 47.15.G-

INTRODUCTION

Shear flows past bubbles and droplets adhering to a solid surface are relevant situations arising in a wide range of applications, engineering problems, physiological and natural phenomena [1]. As an example we can cite bubble growth and detachment from a heated wall [2, 3], drop removal and dislocation in detergency problems [4] and also membrane emulsification, where a liquid is pumped into another, shearing droplets and consequently forming emulsions. Pertinent physiological applications can also be included such as the growth of thrombosis and the deformation and dislodging of white and red blood cells adhering to the endothelium. In all these cases, mathematical modelling and precise quantitative solutions are necessary to exactly quantify the properties of the flow. Previous works and studies considered shear flows over protuberances, such as the work of O'Neill [5] who derived an infinite series solution for the flow over a full sphere in contact with a wall, as well as the papers of Hyman [6] and Price [7] who derived a solution for the case of hemispherical no-slip bumps, a problem which can be considered as a limiting case for highly viscous droplets. Pozrikidis [8] derived a series of solutions for oblate hemispheroidal protuberances with the boundary element method. A number of researchers have also considered problems connected with drop displacement, a fundamental issue that has been discussed in a series of papers by Dussan and coworkers [9, 10, 11] and by Dimitrakopoulos and Higdon [12, 13]. In other works, also some variations on the drop displacement problem have been investigated such as the works of Yon, Li and Pozrikidis [14, 15] who studied shear induced deformations of droplets with fixed contact lines and the work of Schleizer [16] who faced the problem of droplet displacement in both pressure driven and shear flows. More recently also inertial effects past pinned droplets have been considered in the work of Spelt [17]. In this paper we derive an exact solution for the case of an incompressible shear flow over a hemispherical droplet of arbitrary viscosity. This solution will be quantified as a function of the viscosity ratio between the droplet and the fluid and is the natural generalization of the one proposed by Price [7], here recovered in the limit of highly viscous droplet. Several analytical expressions including the force and torque acting on the droplet will be given. Moreover, in the limit of small Capillary numbers, the role of surface deformations will be investigated and comparison with available data will be presented. Results here reported are also useful to formulate effective boundary condition problems [18, 19, 20, 21], an issue which has been recently renewed due to its relevance in small scale hydrodynamics [22] and its possible connections with laminar drag reduction mechanisms [23, 24, 25, 26, 27, 28].

FORMULATION OF THE PROBLEM

We consider the motion of a viscous incompressible fluid with velocity \mathbf{v} , of constant density ρ and viscosity η , close to a solid plane boundary. Under the assumption of small Reynolds numbers, this motion is reasonably approximated by a uniform shear flow whose magnitude will be denoted with S . We will consider how this flow is disturbed by a hemispherical drop of radius R and density $\hat{\rho}$ on the plane boundary. We will use polar coordinates (r, θ, ϕ) with the origin in the center of the hemisphere and an x -axis in the direction of the shear flow (see figure 1 for details). The flow inside the drop will be identified with a velocity $\hat{\mathbf{v}}$ and viscosity $\hat{\eta}$ in a prescribed ratio with respect to the outer viscosity. This ratio will be denoted by $\chi = \hat{\eta}/\eta$. Indicating with p and \hat{p} the outer and inner pressure respectively, the continuity and Stokes equations read as follows:

$$\nabla \cdot \mathbf{v} = \nabla \cdot \hat{\mathbf{v}} = 0, \quad (1)$$

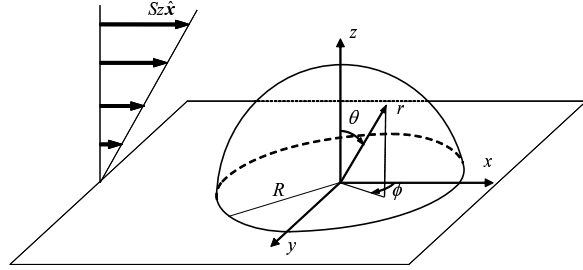


FIG. 1: Configuration for the problem

$$\nabla \cdot \boldsymbol{\sigma} = \nabla \cdot \hat{\boldsymbol{\sigma}} = 0, \quad (2)$$

where

$$\boldsymbol{\sigma} = -p\mathbf{I} + \eta (\nabla \mathbf{v} + (\nabla \mathbf{v})^T), \quad \hat{\boldsymbol{\sigma}} = -\hat{p}\mathbf{I} + \hat{\eta} (\nabla \hat{\mathbf{v}} + (\nabla \hat{\mathbf{v}})^T). \quad (3)$$

We will assume no-slip boundary conditions on the wall:

$$\mathbf{v} = 0 \quad r \geq R, \theta = \frac{\pi}{2}, 0 \leq \phi \leq 2\pi, \quad (4)$$

$$\hat{\mathbf{v}} = 0 \quad r \leq R, \theta = \frac{\pi}{2}, 0 \leq \phi \leq 2\pi, \quad (5)$$

and, on the interface of the hemispherical bump ($r = R, 0 \leq \theta \leq \frac{\pi}{2}, 0 \leq \phi \leq 2\pi$), we should match the inner and outer solutions by imposing (i) the kinetic condition for two phases, (ii) the continuity of the tangential velocity in two directions and (iii) the continuity of the shearing surface force per unit area in two directions. These boundary conditions are written in a general form:

$$\begin{aligned} \mathbf{e}_r \cdot \mathbf{v} &= \mathbf{e}_r \cdot \hat{\mathbf{v}} = 0, \\ \mathbf{e}_r \times \mathbf{v} &= \mathbf{e}_r \times \hat{\mathbf{v}}, \\ \mathbf{e}_r \times \{\boldsymbol{\sigma} \cdot \mathbf{e}_r\} &= \mathbf{e}_r \times \{\hat{\boldsymbol{\sigma}} \cdot \mathbf{e}_r\}, \end{aligned} \quad (6)$$

with \mathbf{e}_r the radial normal unit vector at the bump surface.

GENERAL SOLUTION

In the subsequent developments we will assume that all variables have been non-dimensionalized using S, ρ, η in the outer region and $S, \hat{\rho}, \hat{\eta}$ in the inner region together with a reference length scale given by the radius of the drop R . We will also introduce the disturbances of the velocity vectors \mathbf{v} and $\hat{\mathbf{v}}$ from the linear shear flow as

$$\mathbf{q} = \mathbf{e}_x z - \mathbf{v}, \quad \hat{\mathbf{q}} = \mathbf{e}_x z - \hat{\mathbf{v}}. \quad (7)$$

These disturbances satisfy the continuity and Stokes equations:

$$\nabla \cdot \mathbf{q} = \nabla \cdot \hat{\mathbf{q}} = 0, \quad (8)$$

$$\nabla^2 \mathbf{q} = -\nabla p \quad \nabla^2 \hat{\mathbf{q}} = -\nabla \hat{p}. \quad (9)$$

The boundary conditions for non slip walls are now expressed by

$$\mathbf{q} = 0 \quad r \geq 0, \theta = \frac{\pi}{2}, 0 \leq \phi \leq 2\pi, \quad (10)$$

while, considering the shear velocity $\mathbf{e}_x z$ written in spherical coordinates, we can rewrite the boundary conditions (6) using the disturbance velocities as

$$\begin{aligned} q_r - \cos \theta \sin \theta \cos \phi &= 0, \quad \hat{q}_r - \cos \theta \sin \theta \cos \phi = 0, \quad q_\theta = \hat{q}_\theta, \quad q_\phi = \hat{q}_\phi, \\ \frac{\partial q_\theta}{\partial r} - q_\theta &= \chi \left(\frac{\partial \hat{q}_\theta}{\partial r} - \hat{q}_\theta \right), \quad \frac{\partial q_\phi}{\partial r} - q_\phi = \chi \left(\frac{\partial \hat{q}_\phi}{\partial r} - \hat{q}_\phi \right) \\ r &= 1, 0 \leq \theta \leq \pi/2, 0 \leq \phi \leq 2\pi. \end{aligned} \quad (11)$$

To reduce the ϕ -dependence of the boundary conditions (11) we introduce $u, v, w, \hat{u}, \hat{v}$ and \hat{w} given by

$$u = \frac{q_r}{\cos \phi}, \quad v = \frac{q_\theta}{\cos \phi}, \quad w = \frac{q_\phi}{\sin \phi}, \quad \hat{u} = \frac{\hat{q}_r}{\cos \phi}, \quad \hat{v} = \frac{\hat{q}_\theta}{\cos \phi}, \quad \hat{w} = \frac{\hat{q}_\phi}{\sin \phi}. \quad (12)$$

We further introduce U, V and W as functions of the velocity components u, v and w :

$$U = u \sin \theta + v \cos \theta + w, \quad V = u \sin \theta + v \cos \theta - w, \quad W = u \cos \theta - v \sin \theta, \quad (13)$$

and, for the inner region, \hat{U}, \hat{V} and \hat{W} are similarly defined. Then, the boundary conditions on the droplet surface can be rewritten using $U, V, W, \hat{U}, \hat{V}$ and \hat{W} as

$$W \cos \theta + \left(\frac{U + V}{2} \right) \sin \theta - \cos \theta \sin \theta = 0, \quad (14)$$

$$\hat{W} \cos \theta + \left(\frac{\hat{U} + \hat{V}}{2} \right) \sin \theta - \cos \theta \sin \theta = 0, \quad (15)$$

$$-W \sin \theta + U \cos \theta = -\hat{W} \sin \theta + \hat{U} \cos \theta, \quad (16)$$

$$-W \sin \theta + V \cos \theta = -\hat{W} \sin \theta + \hat{V} \cos \theta, \quad (17)$$

$$\left(\frac{\partial}{\partial r} - 1 \right) \{-W \sin \theta + U \cos \theta\} = \chi \left(\frac{\partial}{\partial r} - 1 \right) (-\hat{W} \sin \theta + \hat{U} \cos \theta), \quad (18)$$

$$\left(\frac{\partial}{\partial r} - 1 \right) (-W \sin \theta + V \cos \theta) = \chi \left(\frac{\partial}{\partial r} - 1 \right) (-\hat{W} \sin \theta + \hat{V} \cos \theta). \quad (19)$$

As for the pressure field, we define P and \hat{P} as

$$P = -\frac{p}{\cos \phi}, \quad \hat{P} = -\frac{\hat{p}}{\cos \phi}. \quad (20)$$

Since in the creeping flow approximation the pressure is harmonic, we can give a non divergent solution in a series of the associated Legendre functions P_n^m :

$$P = \sum_{n=1}^{\infty} \frac{A_n P_n^1(\mu)}{r^{n+1}}, \quad \hat{P} = \sum_{n=1}^{\infty} \hat{A}_n r^n P_n^1(\mu), \quad (21)$$

where $\mu = \cos \theta$ and A_n, \hat{A}_n are unknown constants to be determined with the boundary conditions. Here we employ the definition of the associated Legendre functions defined in terms of the polynomials of zeroth order as $P_n^m(x) = (1 - x^2)^{m/2} d^m P_n(x) / dx^m$ (e.g. $P_1^1(\cos \theta) = \sin \theta$). From the Stokes equations (9), we can determine the

general solutions in the expansion form

$$\begin{aligned} W &= \sum_{n=1}^{\infty} \frac{nA_n}{2(2n+1)r^n} P_{n+1}^1(\mu) + \sum_{n=2}^{\infty} \frac{C_n}{r^n} P_{n-1}^1(\mu), \\ U &= \sum_{n=1}^{\infty} \frac{A_n}{2(2n+1)r^n} P_{n+1}^2(\mu) + \sum_{n=3}^{\infty} \frac{E_n}{r^n} P_{n-1}^2(\mu), \\ V &= - \sum_{n=1}^{\infty} \frac{n(n+1)A_n}{2(2n+1)r^n} P_{n+1}(\mu) + \sum_{n=1}^{\infty} \frac{G_n}{r^n} P_{n-1}(\mu), \end{aligned} \quad (22)$$

$$\begin{aligned} \hat{W} &= \sum_{n=2}^{\infty} \frac{(n+1)\hat{A}_n r^{n+1}}{2(2n+1)} P_{n-1}^1(\mu) + \sum_{n=0}^{\infty} \hat{C}_n r^{n+1} P_{n+1}^1(\mu), \\ \hat{U} &= - \sum_{n=3}^{\infty} \frac{\hat{A}_n r^{n+1}}{2(2n+1)} P_{n-1}^2(\mu) + \sum_{n=1}^{\infty} \hat{E}_n r^{n+1} P_{n+1}^2(\mu), \\ \hat{V} &= \sum_{n=1}^{\infty} \frac{n(n+1)\hat{A}_n r^{n+1}}{2(2n+1)} P_{n-1}(\mu) + \sum_{n=0}^{\infty} \hat{G}_n r^{n+1} P_{n+1}(\mu), \end{aligned} \quad (23)$$

with C_n , E_n , G_n and \hat{C}_n , \hat{E}_n , \hat{G}_n additional constants. Upon using the no-slip boundary condition on the plane wall (10) we get:

$$C_{2n} = \frac{2n+1}{2(4n+1)} A_{2n}, \quad E_{2n-1} = \frac{(2n+1)A_{2n-1}}{4(n-1)(4n-1)}, \quad G_{2n-1} = -\frac{(2n-1)^2 A_{2n-1}}{2(4n-1)}, \quad (24)$$

$$\hat{C}_{2n} = \frac{n\hat{A}_{2n}}{4n+1}, \quad \hat{E}_{2n-1} = -\frac{(n-1)\hat{A}_{2n-1}}{(2n+1)(4n-1)}, \quad \hat{G}_{2n-1} = \frac{2n^2 \hat{A}_{2n-1}}{4n-1}, \quad (25)$$

and, imposing the continuity equation (8) together with (10), we find:

$$C_{2n-1} = \frac{(2n-1)(2n+1)}{4(4n-1)(n-1)} A_{2n-1},$$

$$E_{2n} = \frac{1}{2(n-1)(2n-1)} \left\{ \frac{(2n-3)(2n+1)}{4n+1} A_{2n} + G_{2n} \right\},$$

$$\hat{C}_{2n-1} = \frac{2n(n-1)}{(2n+1)(4n-1)} \hat{A}_{2n-1},$$

$$\hat{E}_{2n} = \frac{1}{2(n+1)(2n+3)} \left\{ -\frac{4n(n+2)}{4n+1} \hat{A}_{2n} + \hat{G}_{2n} \right\},$$

while, for the low-order coefficients, we obtain

$$A_1 = G_1 = \hat{E}_1 = \hat{C}_0 = \hat{C}_1 = 0,$$

and

$$\hat{A}_1 \neq 0, \quad \hat{G}_0 \neq 0.$$

Using these relations, we can rewrite (22) as

$$\begin{aligned} W &= \sum_n \left[\left(\frac{(n-1)A_{2n-2}}{(4n-3)r^{2n-2}} + \frac{(2n+1)A_{2n}}{2(4n+1)r^{2n}} \right) P_{2n-1}^1(\mu) \right. \\ &\quad \left. + \left(\frac{(2n-1)A_{2n-1}}{2(4n-1)r^{2n-1}} + \frac{(2n+1)(2n+3)A_{2n+1}}{4n(4n+3)r^{2n+1}} \right) P_{2n}^1(\mu) \right], \end{aligned} \quad (26)$$

$$U = \sum_n \left[\left(\frac{A_{2n-2}}{2(4n-3)r^{2n-2}} + \frac{(2n-3)(2n+1)A_{2n}}{2(n-1)(2n-1)(4n+1)r^{2n}} + \frac{G_{2n}}{2(n-1)(2n-1)r^{2n}} \right) P_{2n-1}^2(\mu) \right. \\ \left. + \left(\frac{A_{2n-1}}{2(4n-1)r^{2n-1}} + \frac{(2n+3)A_{2n+1}}{4n(4n+3)r^{2n+1}} \right) P_{2n}^2(\mu) \right], \quad (27)$$

$$V = \sum_n \left[\left(-\frac{(n-1)(2n-1)A_{2n-2}}{(4n-3)r^{2n-2}} + \frac{G_{2n}}{r^{2n}} \right) P_{2n-1}(\mu) \right. \\ \left. + \left(-\frac{n(2n-1)A_{2n-1}}{(4n-1)r^{2n-1}} - \frac{(2n+1)^2 A_{2n+1}}{2(4n+3)r^{2n+1}} \right) P_{2n}(\mu) \right], \quad (28)$$

while, for the inner region, we can rewrite (23) as

$$\hat{W} = \sum_n \left[\left(\frac{(2n+1)\hat{A}_{2n}r^{2n+1}}{2(4n+1)} + \frac{(n-1)\hat{A}_{2n-2}r^{2n-1}}{4n-3} \right) P_{2n-1}^1(\mu) \right. \\ \left. + \left(\frac{(n+1)\hat{A}_{2n+1}r^{2n+2}}{4n+3} + \frac{2n(n-1)\hat{A}_{2n-1}r^{2n}}{(2n+1)(4n-1)} \right) P_{2n}^1(\mu) \right], \quad (29)$$

$$\hat{U} = \sum_n \left[\left(-\frac{\hat{A}_{2n}r^{2n+1}}{2(4n+1)} - \frac{2(n-1)(n+1)\hat{A}_{2n-2}r^{2n-1}}{n(2n+1)(4n-3)} + \frac{\hat{G}_{2n-2}r^{2n-1}}{2n(2n+1)} \right) P_{2n-1}^2(\mu) \right. \\ \left. + \left(-\frac{\hat{A}_{2n+1}r^{2n+2}}{2(4n+3)} - \frac{(n-1)\hat{A}_{2n-1}r^{2n}}{(2n+1)(4n-1)} \right) P_{2n}^2(\mu) \right], \quad (30)$$

$$\hat{V} = \sum_n \left[\left(\frac{n(2n+1)\hat{A}_{2n}r^{2n+1}}{4n+1} + \hat{G}_{2n-2}r^{2n-1} \right) P_{2n-1}(\mu) \right. \\ \left. + \left(\frac{(n+1)(2n+1)\hat{A}_{2n+1}r^{2n+2}}{4n+3} + \frac{2n^2\hat{A}_{2n-1}r^{2n}}{4n-1} \right) P_{2n}(\mu) \right]. \quad (31)$$

In the previous expressions the six unknown set of coefficients A_{2n+1} , A_{2n} , G_{2n} , \hat{A}_{2n-1} , \hat{A}_{2n} and \hat{G}_{2n-2} with $n \geq 1$ have now to be determined by the imposition of the six conditions (14)-(19) on the hemispherical bump.

Determination of the coefficients

To determine the coefficients A_{2n+1} , A_{2n} , G_{2n} , \hat{A}_{2n-1} , \hat{A}_{2n} and \hat{G}_{2n-2} for $n \geq 1$, we need recurrence formulae that can be deduced from the boundary conditions at $r = 1$ given by (14)-(19). These recurrence formulae are given in the appendix and, although they are written as infinite series, we numerically solve the problem by truncating the system of equations determining the coefficients. For each of the six coefficients we consider modes up to $n = 100$ and to have a good indication of the accuracy of this procedure, the numerically estimated coefficients are substituted into (14)-(19) until the boundary conditions are satisfied to at least five decimal places. The coefficients A_{2n+1} , A_{2n} , G_{2n} , \hat{A}_{2n-1} , \hat{A}_{2n} and \hat{G}_{2n-2} up to $n = 15$ are listed in tables I-V for $\chi = 0, 0.1, 1, 10$ and 10^{100} . In figure 2 we show the kinematical structure of the flow and the development of stagnation points and flow reversal. Let us notice that for high viscosity ratio the streamlines plot is consistent with what obtained by Pozrikidis [8].

It is now useful to check the validity for two extreme limits $\chi \rightarrow 0$ and $\chi \rightarrow \infty$. For the free-slip bump $\chi = 0$, as also confirmed by our numerical solution shown in Table I, the solution is analytical and can be expressed as

$$A_n = \frac{2}{3}\delta_{n2}, \quad G_n = \frac{2}{5}\delta_{n2}. \quad (32)$$

Using this solution, we determine U , V , W and P

$$W = \frac{\sqrt{1-\mu^2}\mu^2}{r^2}, \quad U = \frac{(1-\mu^2)\mu}{r^2}, \quad V = \frac{(1-\mu^2)\mu}{r^2}, \\ P = \frac{2\sqrt{1-\mu^2}\mu}{r^3}. \quad (33)$$

The velocity field around the hemisphere is then given by

$$\mathbf{v} = \mathbf{e}_r \left(r - \frac{1}{r^2} \right) \cos \theta \sin \theta \cos \phi + \mathbf{e}_\theta r \cos^2 \theta \cos \phi - \mathbf{e}_\phi r \cos \theta \sin \phi \quad (34)$$

that can also be rewritten together with the pressure in Cartesian coordinates

$$\begin{aligned} \mathbf{v} &= \mathbf{e}_x \left(z - \frac{x^2 z}{r^5} \right) - \mathbf{e}_y \frac{xyz}{r^5} - \mathbf{e}_z \frac{xz^2}{r^5}, \\ p &= - \frac{2xz}{r^5}. \end{aligned} \quad (35)$$

It should be noted that the present solution (35) is same as the flow around a free-slip sphere in an infinite fluid. It is because the presence of the free-slip sphere does not alter the θ and ϕ components of the velocity vector from the uniform shear flow and then the modulated velocity becomes zero at $z = 0$.

In the case of the largest viscosity ratio $\chi = 10^{100}$, the coefficients A_{2n+1} , A_{2n} and G_{2n} listed in Table V show quantitative agreement with those for the no-slip bump shown in the paper by Price [7]. The inner solution is analytical and given by $\hat{A}_n = 0$ and $\hat{G}_n = 2\delta_{0n}$ that imply a zero velocity inside the bump.

Torque and Force

We now evaluate the force and the torque acting on the hemisphere for various viscosity ratios. The general strategy will be to write them as a functions of the constants A_{2n} , S_{2n+1} , G_{2n} and then use the coefficients obtained from the numerical solution in the previous section in order to evaluate them. To do this, we write the force \mathbf{F} and the torque \mathbf{T} in the most general form

$$\mathbf{F} = \int_0^{2\pi} d\phi \int_0^{\pi/2} d\theta \sin \theta (\boldsymbol{\sigma} \cdot \mathbf{e}_r)_{r=1}, \quad (36)$$

$$\mathbf{T} = \int_0^{2\pi} d\phi \int_0^{\pi/2} d\theta \sin \theta [r \mathbf{e}_r \times (\boldsymbol{\sigma} \cdot \mathbf{e}_r)]_{r=1}. \quad (37)$$

Let us notice that the symmetry of the system with respect to ϕ is such that only the x component of the force vector F_x and y component of the torque vector T_y are non-zero. To estimate these components, considering the kinetic condition in (11) and using U , V and W given by the general solution we can exactly express the torque and force as a function of A_{2n} , A_{2n+1} and G_{2n} :

$$F_x = \pi \left[\frac{1}{2} + \frac{4}{5} A_3 - \sum_{n=1}^{\infty} \frac{(-1)^n (2n+1)!!}{(2n-3)(2n-1)(2n-2)!!} \left(\frac{(4n^3 - 9n - 2) A_{2n}}{2(n+1)(4n+1)} + \frac{(2n^2 - 3n - 1) G_{2n}}{n(2n+1)} \right) \right], \quad (38)$$

$$T_y = \pi \left[-\frac{3}{5} A_2 + G_2 + \sum_{n=1}^{\infty} \frac{(-1)^n (2n+1)!!}{(2n-1)(2n)!!} A_{2n+1} \right], \quad (39)$$

with

$$(2n+1)!! = (2n+1) \times (2n-1) \times \dots \times 1, \quad (2n)!! = (2n) \times (2n-2) \times \dots \times 2, \quad 0!! = 1.$$

In the limit of highly viscous droplet ($\chi \rightarrow \infty$), from the numerical evaluation of the coefficients for $\chi = 10^{100}$ (see Table V) we determine the force and torque as

$$F_x = 4.30322\pi, \quad T_y = 2.44132\pi, \quad (40)$$

and both results are consistent with the evaluations $F_x = 4.30\pi$, $T_y = 2.44\pi$ for the rigid no-slip bump given in the paper by Price [7].

The profiles of F_x and T_y as a function of χ are respectively shown in Figure 3 and Figure 4. As it is clearly shown

both the torque and the force approach a finite value for very small ($\chi \rightarrow 0$) and large ($\chi \rightarrow \infty$) viscosity ratio. Considering these asymptotic behaviors, we can estimate

$$\frac{F_x}{\pi} \approx \frac{2 + 4.51003\chi}{1 + 1.04806\chi}, \quad (41)$$

$$\frac{T_y}{\pi} \approx \frac{2.18808\chi}{1 + 0.896271\chi}, \quad (42)$$

in which the numerical coefficients have been determined from the method of least squares.

Effects of Capillary number on deformation

In this section we investigate the local difference of the normal stress between the inner and outer regions of the bump. Further, we evaluate the deformation of the bump consistently with the Laplace law [29, 30] resting on the assumption that these deformations are small. To do this we have to introduce the Capillary number as

$$Ca = \frac{\eta S R_0}{\gamma}, \quad (43)$$

where R_0 , S and γ are dimensional length, shear and surface tension scales. Next we write a dimensional stress tensor as

$$\boldsymbol{\sigma}^{(dim)} = \boldsymbol{\sigma} S \eta - P_s, \quad (44)$$

$$\hat{\boldsymbol{\sigma}}^{(dim)} = \hat{\boldsymbol{\sigma}} S \eta \chi - \hat{P}_s, \quad (45)$$

where the contributions $\boldsymbol{\sigma}$ and $\hat{\boldsymbol{\sigma}}$ are purely dimensionless, i.e. they correspond to a unitary shear S and unitary viscosity η described in the previous sections. The terms P_s and \hat{P}_s represent constant dimensional background pressures, i.e. the pressure inside/outside the bump in absence of flow. Assuming $Ca \ll 1$, if we indicate with $r = R$ the position of the interface, we should write:

$$R(\theta, \phi) = R_0(1 + CaR^{(1)}(\theta, \phi) + \mathcal{O}(Ca^2)), \quad (46)$$

where $R^{(1)}$ accounts for the displacement from the pure hemisphere. The Laplace law on the interface is written in a general form

$$\kappa^{(dim)} \gamma = \sigma_{rr}^{(dim)} - \hat{\sigma}_{rr}^{(dim)}, \quad (47)$$

where $\kappa^{(dim)} = \frac{\kappa}{R_0}$ denotes the dimensional curvature, with κ its dimensionless counterpart. If $Ca \ll 1$, the displacement is small enough and the curvature on the bump interface is given by

$$\begin{aligned} \kappa &= R_0 \left\{ \nabla \cdot \left(\frac{\nabla(r - R)}{|\nabla(r - R)|} \right) \right\}_{r=R} \approx R_0 \left\{ \nabla^2(r - R) \right\}_{r=R} \\ &= \frac{2}{1 + CaR^{(1)} + \dots} - \left[\frac{1}{\sin \theta} \frac{\partial}{\partial \theta} \left(\sin \theta \frac{\partial}{\partial \theta} \right) + \frac{1}{\sin^2 \theta} \frac{\partial^2}{\partial \phi^2} \right] CaR^{(1)} + \dots \\ &= 2Ca^0 - Ca^1 \left[2 + \frac{1}{\sin \theta} \frac{\partial}{\partial \theta} \left(\sin \theta \frac{\partial}{\partial \theta} \right) + \frac{1}{\sin^2 \theta} \frac{\partial^2}{\partial \phi^2} \right] R^{(1)} + \mathcal{O}(Ca^2), \end{aligned} \quad (48)$$

hence $\frac{\kappa}{Ca} = (\sigma_{rr} - \chi \hat{\sigma}_{rr})_{r=1} + (\hat{P}_s - P_s)/(S\eta)$ and

$$\frac{2}{Ca} - \left[2 + \frac{1}{\sin \theta} \frac{\partial}{\partial \theta} \left(\sin \theta \frac{\partial}{\partial \theta} \right) + \frac{1}{\sin^2 \theta} \frac{\partial^2}{\partial \phi^2} \right] R^{(1)} + \mathcal{O}(Ca^1) = (\sigma_{rr} - \chi \hat{\sigma}_{rr})_{r=1} + (\hat{P}_s - P_s)/(S\eta). \quad (49)$$

In the absence of the shear flow, the pressure is constant inside and outside the bump and equal to \hat{P}_s and P_s respectively. The gap between the two pressures is determined by $(\hat{P}_s - P_s)/(S\eta) = 2Ca^{-1}$ from the $\mathcal{O}(Ca^{-1})$ of (49). This means that in presence of a non zero velocity, in order to find consistency with the Laplace law, we should

consider a finite displacement given by a non zero $R^{(1)}$ in (46). To determine this displacement, we should solve the $\mathcal{O}(Ca^0)$ in (49):

$$-\left[2 + \frac{1}{\sin \theta} \frac{\partial}{\partial \theta} \left(\sin \theta \frac{\partial}{\partial \theta}\right) + \frac{1}{\sin^2 \theta} \frac{\partial^2}{\partial \phi^2}\right] R^{(1)} = (\sigma_{rr} - \chi \hat{\sigma}_{rr})_{r=1}, \quad (50)$$

with the boundary condition

$$R^{(1)} = 0 \quad \text{at} \quad \theta = \frac{\pi}{2}, 0 \leq \phi \leq 2\pi. \quad (51)$$

If we write the normal stress jump in the expansion form with respect to the associated Legendre polynomials

$$(\sigma_{rr} - \chi \hat{\sigma}_{rr})_{r=1} = \sum_{n=1}^{\infty} Q_n P_n^1(\mu) \cos \phi, \quad (52)$$

the expansion coefficients Q_n can be determined as:

$$\begin{aligned} Q_{2n} = & \frac{2\delta_{1n}}{3}(1-\chi) + \frac{4n^2 + 6n - 1}{4n - 1} A_{2n} + \frac{2(n+1)^2(2n+3)(8n^2 + 6n - 3)}{n(2n+1)(4n+3)(4n+5)} A_{2n+2} + \frac{2(n+1)}{n(2n+1)} G_{2n+2} \\ & + \chi \left(\frac{2(n-1)(2n-1)^2(4n^2 + n - 2)}{n(2n+1)(4n-3)(4n-1)} \hat{A}_{2n-2} + \frac{4n^2 - 2n - 3}{4n+3} \hat{A}_{2n} + \frac{2n-1}{n(2n+1)} \hat{G}_{2n-2} \right), \end{aligned} \quad (53)$$

$$\begin{aligned} Q_{2n-1} = & \frac{4n^2 + 2n - 3}{4n - 3} A_{2n-1} + \frac{(n+1)(2n+1)^2}{n(4n+1)} A_{2n+1} \\ & + \chi \left(\frac{4(n-1)^2(2n-3)}{(2n-1)(4n-3)} \hat{A}_{2n-3} + \frac{4n^2 - 6n - 1}{4n+1} \hat{A}_{2n-1} \right). \end{aligned} \quad (54)$$

We now solve (50) and determine the displacement

$$R^{(1)} = \left(\frac{R_0^{(1)} \sqrt{1-\mu^2}}{1+\mu} + \sum_{n=2}^{\infty} R_n^{(1)} P_n^1(\mu) \right) \cos \phi, \quad (55)$$

where

$$R_0^{(1)} = \sum_{k=2}^{\infty} \frac{(-1)^k (2k-1)!!}{2(k-1)(2k+1)(2k-2)!!} Q_{2k-1}, \quad (56)$$

$$R_n^{(1)} = \frac{Q_n}{(n-1)(n+2)} \quad \text{for} \quad n \geq 2. \quad (57)$$

Concerning the ϕ dependence of the normal stress jump, this is simply proportional to $\cos \phi$. In figure 5 we show the deformation of the bump on the plane of $y = 0$ with a Capillary number $Ca = 0.05$. These deformations have been estimated from (55), (56) and (57) with the numerical coefficients in (53) and (54) determined with the procedure of the previous section. Moreover, to better quantify the role of deformations with respect to the hemispherical bump, advancing and receding contact angles should be respectively defined by $\pi/2 + \Delta\theta$ and $\pi/2 - \Delta\theta$, with $\Delta\theta$ proportional to Ca if the deformation is small enough (see figure 6). For various viscosity ratios χ , $\Delta\theta/Ca$ is then plotted in figure 7. Considering the asymptotic behaviors, this deformation can be approximated by

$$\Delta\theta \approx \frac{(2 + 7.07185\chi)}{(1 + 0.908826\chi)} Ca, \quad (58)$$

in which the numerical coefficients have been determined from the method of least squares.

For the case of hemispherical droplet whose viscosity is equal to the surrounding fluid ($\chi = 1$), it is instructive to compare our results with the ones of Li and Pozrikidis [15]. In figure 8 we plot the deformation parameter $D = \frac{A-B}{A+B}$ as a function of the Capillary number. A and B are, respectively, the maximum and minimum radial distances of the interface from the origin. Note that the corresponding slope for a spherical drop suspended in an infinite simple shear

flow is equal to 35/32 [31] and suggests that the wall is promoting the deformation of the drop as it is also confirmed by the computation of Li and Pozrikidis [15] (see their figure 6 (e)) with the boundary integral method. To further compare our results with the ones of Li and Pozrikidis, in figure 9 we plot the advancing and receding contact angles as a function of the Capillary number and a good agreement is found.

The numerical investigations of Li and Pozrikidis [15] were also extended in another paper by Yon and Pozrikidis [14] by examining the role played by the viscosity ratio. In particular in figure 10 we compare our result for the advancing contact angle as a function of the Capillary number with the numerical results shown in figure 3 (g) of the paper by Yon and Pozrikidis and quantitative agreement is found.

CONCLUSIONS

A solution based on an infinite series expansion for the case of a linear shear flow past a hemispherical droplet with arbitrary viscosity has been explicitly constructed. The procedure here proposed closely follows the one used in an earlier paper by Price [7] who investigated the case of a hemispherical no-slip bump, here recovered in the limiting situation of highly viscous droplet. Several expressions including the torque and force acting on the hemisphere are exactly derived and computed as a function of the viscosity ratio. The role of deformations on the hemispherical surface has also been investigated in the limit of small Capillary numbers and a comparison with available results has been presented. Besides providing the exact structure of the flow and its averaged properties around the drop, results here reported are also relevant in the formulation of effective boundary conditions for Stokes flows over surfaces made up of prescribed distributions of droplets.

In this appendix we report the recurrence formulae to determine the coefficients A_{2n+1} , A_{2n} , G_{2n} , \hat{A}_{2n-1} , \hat{A}_{2n} and \hat{G}_{2n-2} for $n \geq 1$. The relevant boundary conditions at $r = 1$ are given by (14)-(19). Using the general representations (26)-(31), we can rewrite the boundary conditions and apply definite integrals for Legendre polynomials

$$\int_0^1 d\mu P_{2n-1}^m(\mu) P_{2k-1}^m(\mu) = \frac{\delta_{nk}}{(4k-1)} \frac{(2k-1+m)!}{(2k-1-m)!}, \quad (59)$$

$$\int_0^1 d\mu P_{2n}^m(\mu) P_{2k}^m(\mu) = \frac{\delta_{nk}}{(4k+1)} \frac{(2k+m)!}{(2k-m)!}, \quad (60)$$

$$\int_0^1 d\mu P_{2n}(\mu) P_{2k-1}(\mu) = \frac{(-1)^{n+k} (2n-1)!! (2k-1)!!}{2(2n-2k+1)(n+k)(2n)!!(2k-2)!!}, \quad (61)$$

$$\int_0^1 d\mu P_{2n}^1(\mu) P_{2k-1}^1(\mu) = \frac{(-1)^{n+k} (2n+1)!! (2k-1)!!}{2(2n-2k+1)(n+k)(2n-2)!!(2k-2)!!}, \quad (62)$$

$$\int_0^1 d\mu P_{2n}^2(\mu) P_{2k-1}^2(\mu) = \frac{(-1)^{n+k} (2n+1)!! (2k+1)!!}{2(2n-2k+1)(n+k)(2n-2)!!(2k-4)!!}. \quad (63)$$

In this way, we can eliminate the summation for the even-order mode and we finally obtain the recurrence formulae:

$$\begin{aligned} \frac{\delta_{k1}}{3} = & \frac{(2k+1)}{2(4k-1)} A_{2k} + \frac{(k+1)(2k+3)(8k^2+6k-3)}{2k(2k+1)(4k+3)(4k+5)} A_{2k+2} + \frac{1}{2k(2k+1)} G_{2k+2} \\ & - \Delta_k \sum_{n=1}^{\infty} (n+1) \Lambda_{n,k} A_{2n+1} \end{aligned} \quad (64)$$

$$\begin{aligned} \frac{\delta_{k1}}{3} = & \frac{(k-1)(2k-1)(4k^2+k-2)}{k(2k+1)(4k-3)(4k-1)} \hat{A}_{2k-2} + \frac{k}{4k+3} \hat{A}_{2k} + \frac{1}{2k(2k+1)} \hat{G}_{2k-2} \\ & - \Delta_k \sum_{n=1}^{\infty} (2n-1) \hat{\Lambda}_{n,k} \hat{A}_{2n-1}, \end{aligned} \quad (65)$$

$$\begin{aligned}
& \frac{6k^2 - 7k - 2}{(2k-1)(4k-1)(4k+1)} A_{2k} + \frac{(2k+3)(6k^2 + 5k - 3)}{2k(2k+1)(4k+3)(4k+5)} A_{2k+2} + \frac{1}{(2k-1)(4k-1)} G_{2k} \\
& + \frac{(2k+3)}{2k(2k+1)(4k+3)} G_{2k+2} - \frac{\Delta_k}{(2k-1)(2k+2)} \sum_{n=1}^{\infty} (n-1)(2n+3) \Lambda_{n,k} A_{2n+1} = \\
& = - \frac{(k-1)(6k^2 + k - 4)}{k(2k+1)(4k-3)(4k-1)} \hat{A}_{2k-2} - \frac{6k^2 + 13k + 3}{2(k+1)(4k+1)(4k+3)} \hat{A}_{2k} + \frac{k-1}{k(2k+1)(4k-1)} \hat{G}_{2k-2} \\
& + \frac{1}{2(k+1)(4k+3)} \hat{G}_{2k} + \frac{\Delta_k}{(k+1)(2k-1)} \sum_{n=1}^{\infty} (n-1)(2n+3) \hat{\Lambda}_{n,k} \hat{A}_{2n-1}, \tag{66}
\end{aligned}$$

$$\begin{aligned}
& - \frac{2k^2(2k+1)}{(4k-1)(4k+1)} A_{2k} - \frac{(k+1)(2k+1)(2k+3)}{(4k+3)(4k+5)} A_{2k+2} + \frac{2k}{4k-1} G_{2k} + \frac{2k+1}{4k+3} G_{2k+2} \\
& + \Delta_k \sum_{n=1}^{\infty} n(2n+1) \Lambda_{n,k} A_{2n+1} = \frac{2k(k-1)(2k-1)}{(4k-3)(4k-1)} \hat{A}_{2k-2} + \frac{k(2k+1)^2}{(4k+1)(4k+3)} \hat{A}_{2k} \\
& + \frac{2k}{4k-1} \hat{G}_{2k-2} + \frac{2k+1}{4k+3} \hat{G}_{2k} - 2\Delta_k \sum_{n=1}^{\infty} n(2n+1) \hat{\Lambda}_{n,k} \hat{A}_{2n-1}, \tag{67}
\end{aligned}$$

$$\begin{aligned}
& - \frac{(2k+1)(6k^2 - 7k - 2)}{(2k-1)(4k-1)(4k+1)} A_{2k} - \frac{(2k+3)^2(6k^2 + 5k - 3)}{2k(2k+1)(4k+3)(4k+5)} A_{2k+2} - \frac{(2k+1)}{(2k-1)(4k-1)} G_{2k} \\
& - \frac{(2k+3)^2}{2k(2k+1)(4k+3)} G_{2k+2} + \frac{\Delta_k}{(k+1)(2k-1)} \sum_{n=1}^{\infty} (n-1)(n+1)(2n+3) \Lambda_{n,k} A_{2n+1} = \\
& = \chi \left\{ - \frac{2(k-1)^2(6k^2 + k - 4)}{k(2k+1)(4k-3)(4k-1)} \hat{A}_{2k-2} - \frac{k(6k^2 + 13k + 3)}{(k+1)(4k+1)(4k+3)} \hat{A}_{2k} \right. \\
& \quad \left. + \frac{2(k-1)^2}{k(2k+1)(4k-1)} \hat{G}_{2k-2} + \frac{k}{(k+1)(4k+3)} \hat{G}_{2k} \right\} \\
& \quad + \frac{\chi \Delta_k}{(k+1)(2k-1)} \sum_{n=1}^{\infty} (n-1)(2n-1)(2n+3) \hat{\Lambda}_{n,k} \hat{A}_{2n-1}, \tag{68}
\end{aligned}$$

$$\begin{aligned}
& \frac{2k^2(2k+1)^2}{(4k-1)(4k+1)} A_{2k} + \frac{(k+1)(2k+1)(2k+3)^2}{(4k+3)(4k+5)} A_{2k+2} - \frac{2k(2k+1)}{(4k-1)} G_{2k} - \frac{(2k+1)(2k+3)}{(4k+3)} G_{2k+2} \\
& - 2\Delta_k \sum_{n=1}^{\infty} n(n+1)(2n+1) \Lambda_{n,k} A_{2n+1} = \chi \left\{ \frac{4k(k-1)^2(2k-1)}{(4k-3)(4k-1)} \hat{A}_{2k-2} + \frac{2k^2(2k+1)^2}{(4k+1)(4k+3)} \hat{A}_{2k} \right. \\
& \quad \left. + \frac{4k(k-1)}{4k-1} \hat{G}_{2k-2} + \frac{2k(2k+1)}{4k+3} \hat{G}_{2k} \right\} - 2\chi \Delta_k \sum_{n=1}^{\infty} n(2n-1)(2n+1) \hat{\Lambda}_{n,k} \hat{A}_{2n-1}, \tag{69}
\end{aligned}$$

where we have used

$$\begin{aligned}
\Lambda_{n,k} &= \frac{(-1)^n (2n+1)!!}{2(2n-2k-1)(2n-2k+1)(n+k)(n+k+1)(2n)!!}, \\
\hat{\Lambda}_{n,k} &= \frac{(-1)^n (2n-1)!!}{4(2n-2k-1)(2n-2k+1)(n+k)(n+k+1)(2n-2)!!}, \tag{70}
\end{aligned}$$

and

$$\Delta_k = \frac{(-1)^k (4k+1)(2k-1)!!}{(2k)!!}. \tag{71}$$

We are indebted to Prof. A. Prosperetti for proposing this problem and for his constant suggestions during the preparation of the manuscript. M. S. is grateful to STW (nanomed Programme) for financial support.

TABLE I: Coefficients for $\chi = 0$

n	A_{2n+1}	A_{2n}	G_{2n}	\hat{A}_{2n-1}	\hat{A}_{2n}	\hat{G}_{2n-2}
1	-4.2435×10^{-12}	0.666667	0.40000	-11.47649	2.53882	8.03099
2	-2.3846×10^{-12}	-9.0339×10^{-14}	-2.5928×10^{-13}	-2.13519	0.17201	5.42824
3	1.1579×10^{-12}	-1.8727×10^{-14}	2.8944×10^{-13}	0.24983	-0.071796	0.12475
4	-1.8929×10^{-12}	-7.2444×10^{-14}	-1.8123×10^{-13}	-0.062825	0.036175	-0.082789
5	-2.1743×10^{-13}	1.6780×10^{-14}	2.5391×10^{-13}	0.019726	-0.020377	0.056309
6	-2.7782×10^{-13}	-1.5622×10^{-14}	-2.1449×10^{-13}	-0.0063530	0.012379	-0.039535
7	3.3070×10^{-15}	1.3030×10^{-14}	1.6910×10^{-13}	0.0015681	-0.0079442	0.028544
8	-8.3398×10^{-14}	4.3793×10^{-15}	-2.0627×10^{-13}	0.00024267	0.0053167	-0.021091
9	-7.9357×10^{-15}	3.6435×10^{-14}	9.0663×10^{-14}	-0.00090699	-0.0036784	0.015882
10	-1.8344×10^{-13}	-1.1164×10^{-14}	-1.4936×10^{-13}	0.0011024	0.0026142	-0.012147
11	1.7744×10^{-14}	1.6463×10^{-14}	1.3542×10^{-13}	-0.0011030	-0.0018995	0.0094079
12	-3.0430×10^{-13}	6.7278×10^{-15}	-2.5442×10^{-13}	0.0010260	0.0014061	-0.0073615
13	-2.2858×10^{-13}	1.5070×10^{-14}	7.3790×10^{-14}	-0.00092290	-0.0010573	0.0058075
14	-2.6355×10^{-13}	-1.8224×10^{-14}	-5.9443×10^{-14}	0.00081663	0.00080565	-0.0046107
15	2.3231×10^{-13}	-1.0819×10^{-14}	2.0463×10^{-13}	-0.00071683	-0.00062094	0.0036777

TABLE II: Coefficients for $\chi = 0.1$

n	A_{2n+1}	A_{2n}	G_{2n}	\hat{A}_{2n-1}	\hat{A}_{2n}	\hat{G}_{2n-2}
1	-0.17436	0.84972	0.50983	-10.46143	2.31835	7.49147
2	-0.077633	0.15800	-0.077149	-1.94082	0.15400	4.92646
3	0.012187	0.0094929	-0.0011555	0.22749	-0.064461	0.11746
4	-0.0035702	-0.0046015	0.0023703	-0.057379	0.032545	-0.077592
5	0.0012341	0.0025121	-0.0022646	0.018100	-0.018362	0.052686
6	-0.00042666	-0.0014877	0.0019020	-0.0058827	0.011167	-0.036976
7	0.00011347	0.00093504	-0.0015382	0.0014964	-0.0071731	0.026705
8	0.000013522	-0.00061510	0.0012302	0.00017241	0.0048045	-0.019748
9	-0.000063680	0.00041948	-0.00098250	-0.00079079	-0.0033262	0.014888
10	0.000080443	-0.00029453	0.00078655	0.00097802	0.0023654	-0.011407
11	-0.000082443	0.00021183	-0.00063199	-0.00098504	-0.0017197	0.0088482
12	0.000078085	-0.00015543	0.00050977	0.00091948	0.0012736	-0.0069382
13	-0.000071276	0.00011601	-0.00041261	-0.00082899	-0.00095812	0.0054870
14	0.000063845	-0.000087837	0.00033493	0.00073472	0.00073043	-0.0043687
15	-0.000056630	0.000067335	-0.00027242	-0.00064571	-0.00056322	0.0034961

TABLE III: Coefficients for $\chi = 1$

n	A_{2n+1}	A_{2n}	G_{2n}	\hat{A}_{2n-1}	\hat{A}_{2n}	\hat{G}_{2n-2}
1	-0.97542	1.68344	1.01007	-5.85249	1.31294	5.05033
2	-0.42739	0.87935	-0.40999	-1.06849	0.077130	2.67984
3	0.067950	0.048954	-0.014276	0.12684	-0.033073	0.077672
4	-0.020266	-0.024073	0.017863	-0.032570	0.016955	-0.049837
5	0.0071884	0.013276	-0.015674	0.010543	-0.0096669	0.033457
6	-0.0026054	-0.0079212	0.012751	-0.0035922	0.0059251	-0.023387
7	0.00079580	0.0050080	-0.010168	0.0010494	-0.0038295	0.016889
8	-0.000042750	-0.0033104	0.0080860	-0.000054498	0.0025779	-0.012520
9	-0.00026832	0.0022669	-0.0064524	-0.00033322	-0.0017925	0.0094793
10	0.00038388	-0.0015974	0.0051775	0.00046672	0.0012795	-0.0073022
11	-0.00041078	0.0011527	-0.0041798	-0.00049081	-0.00093345	0.0057059
12	0.00039788	-0.00084839	0.0033941	0.00046853	0.00069351	-0.0045116
13	-0.00036830	0.00063500	-0.0027709	-0.00042837	-0.00052328	0.0036025
14	0.00033312	-0.00048214	0.0022727	0.00038336	0.00040007	-0.0029001
15	-0.00029762	0.00037060	-0.0018715	-0.00033936	-0.00030935	0.0023503

TABLE IV: Coefficients for $\chi = 10$

n	A_{2n+1}	A_{2n}	G_{2n}	\hat{A}_{2n-1}	\hat{A}_{2n}	\hat{G}_{2n-2}
1	-1.83516	2.55162	1.53097	-1.10110	0.25418	2.56548
2	-0.78449	1.64184	-0.68804	-0.19612	0.011796	0.47557
3	0.12819	0.079556	-0.050045	0.023929	-0.0054338	0.018141
4	-0.039327	-0.040886	0.045731	-0.0063205	0.0028862	-0.011069
5	0.014454	0.023098	-0.036923	0.0021199	-0.0016810	0.0072831
6	-0.0055521	-0.013997	0.029024	-0.00076551	0.0010455	-0.0050478
7	0.0019496	0.0089486	-0.022775	0.00025708	-0.00068302	0.0036351
8	-0.00039965	-0.0059665	0.017979	-0.000050954	0.00046375	-0.0026961
9	-0.00027530	0.0041147	-0.014313	-0.000034189	-0.00032475	0.0020468
10	0.00055414	-0.0029172	0.011495	0.000067373	0.00023324	-0.0015835
11	-0.00064763	0.0021163	-0.0093099	-0.000077380	-0.00017109	0.0012443
12	0.00065388	-0.0015652	0.0075980	0.000076998	0.00012775	-0.00099055
13	-0.00062032	0.0011769	-0.0062438	-0.000072149	-0.000096843	0.00079718
14	0.00057041	-0.00089748	0.0051623	0.000065643	0.000074373	-0.00064750
15	-0.00051578	0.00069277	-0.0042910	-0.000058812	-0.000057759	0.00053005

TABLE V: Coefficients for $\chi = 10^{100}$

n	A_{2n+1}	A_{2n}	G_{2n}	\hat{A}_{2n-1}	\hat{A}_{2n}	\hat{G}_{2n-2}
1	-2.04530	2.75543	1.65326	-1.2272×10^{-99}	2.8662×10^{-100}	2.00000
2	-0.86783	1.82575	-0.73104	-2.1696×10^{-100}	1.2213×10^{-101}	5.1794×10^{-100}
3	0.14321	0.084338	-0.063687	2.6733×10^{-101}	-5.8109×10^{-102}	2.1417×10^{-101}
4	-0.044300	-0.044198	0.054743	-7.1196×10^{-102}	3.1280×10^{-102}	-1.2864×10^{-101}
5	0.016436	0.025196	-0.043364	2.4106×10^{-102}	-1.8352×10^{-102}	8.4124×10^{-102}
6	-0.0064047	-0.015350	0.033811	-8.8306×10^{-103}	1.1467×10^{-102}	-5.8150×10^{-102}
7	0.0023185	0.0098491	-0.026427	3.0574×10^{-103}	-7.5171×10^{-103}	4.1832×10^{-102}
8	-0.00054568	-0.0065846	0.020824	-6.9572×10^{-104}	5.1171×10^{-103}	-3.1021×10^{-102}
9	-0.00023620	0.0045508	-0.016566	-2.9333×10^{-104}	-3.5909×10^{-103}	2.3560×10^{-102}
10	0.00056676	-0.0032322	0.013305	6.8908×10^{-104}	2.5837×10^{-103}	-1.8242×10^{-102}
11	-0.00068450	0.0023485	-0.010782	-8.1786×10^{-104}	-1.8982×10^{-103}	1.4350×10^{-102}
12	0.00070095	-0.0017395	0.0088074	8.2541×10^{-104}	1.4194×10^{-103}	-1.1439×10^{-102}
13	-0.00067033	0.0013096	-0.0072468	-7.7965×10^{-104}	-1.0775×10^{-103}	9.2200×10^{-103}
14	0.00061962	-0.00099993	0.0060008	7.1306×10^{-104}	8.2854×10^{-104}	-7.5021×10^{-103}
15	-0.00056237	0.00077279	-0.0049970	-6.4124×10^{-104}	-6.4425×10^{-104}	6.1534×10^{-103}

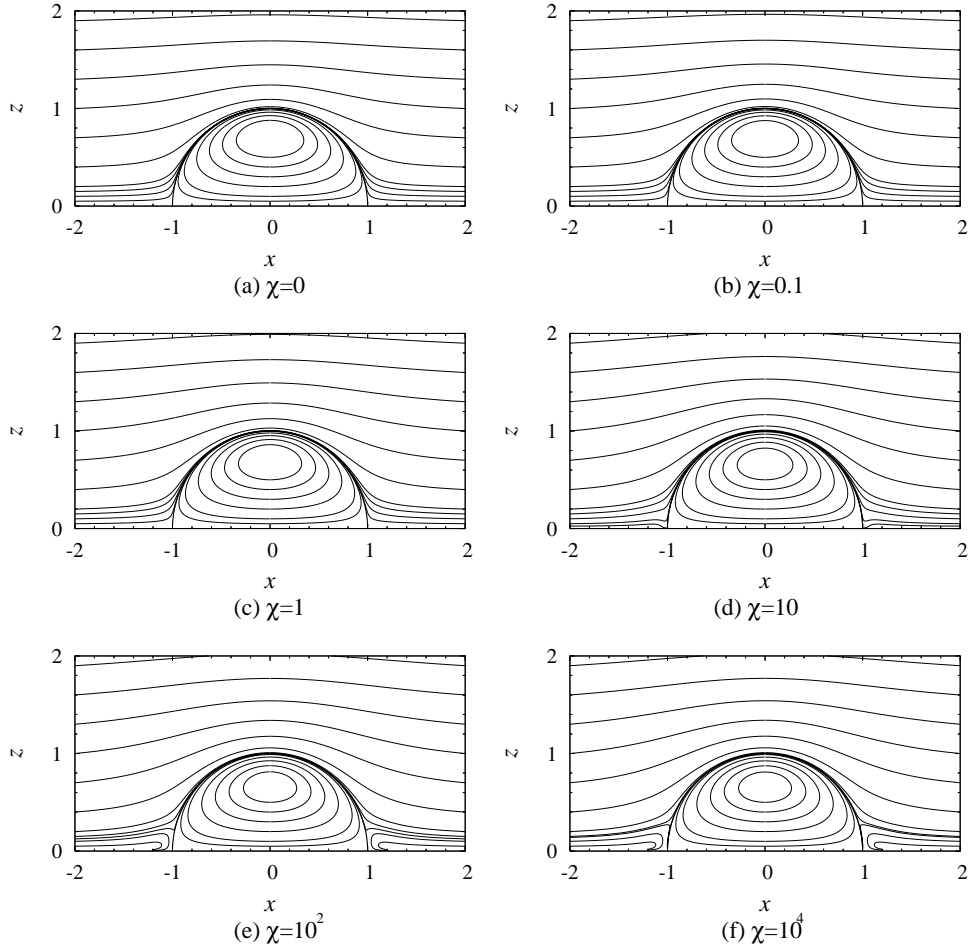


FIG. 2: Streamlines patterns in the in xz mid-plane (for $y = 0$).

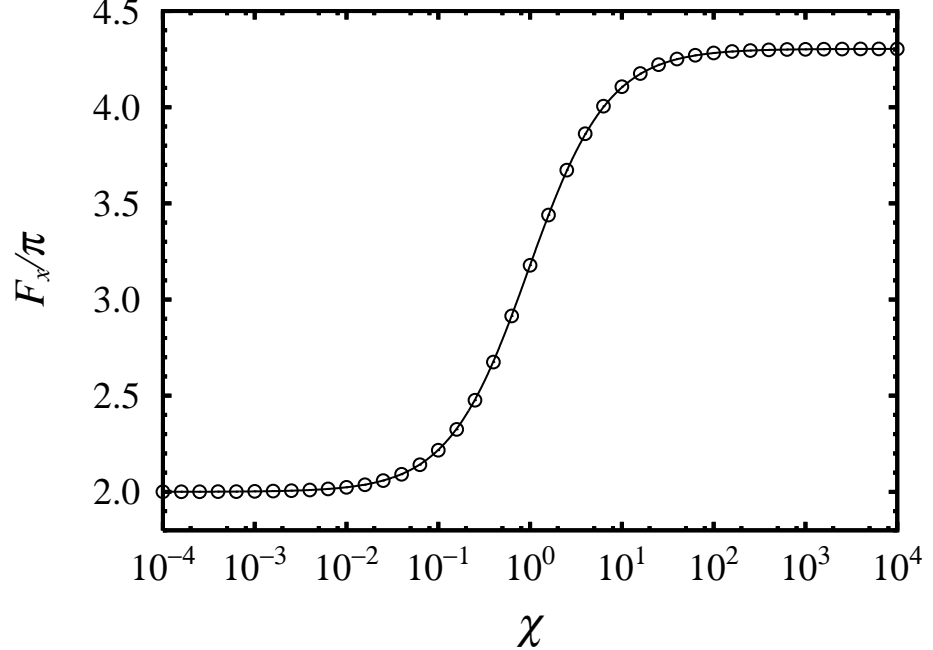


FIG. 3: The force acting on the hemisphere versus the viscosity ratio. The symbol \circ corresponds to the evaluation based on (38). The solid line corresponds to the approximation (41).

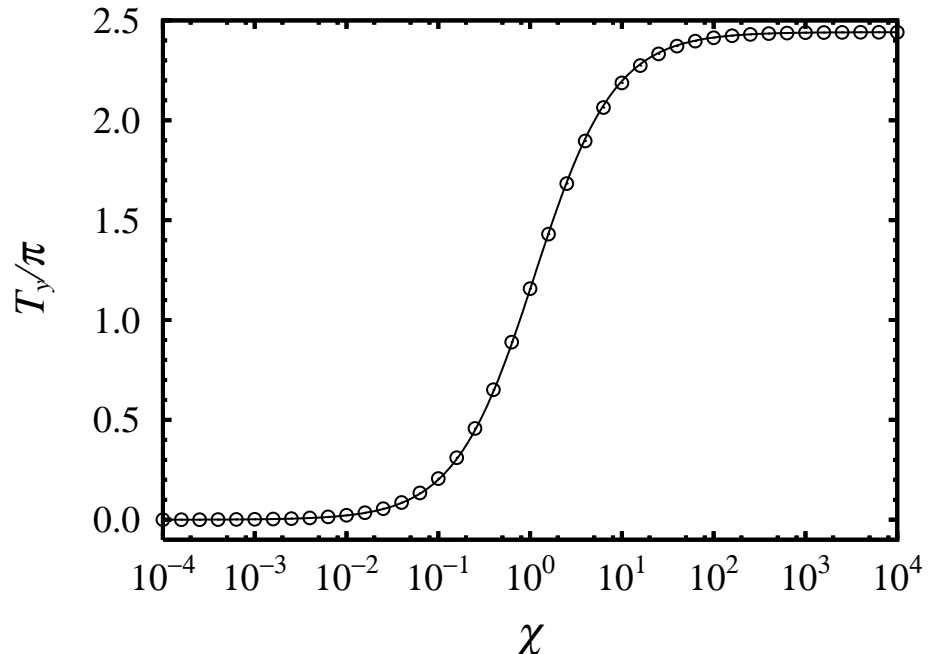


FIG. 4: The torque acting on the hemisphere versus the viscosity ratio. The symbol \circ corresponds to the evaluation based on (39). The solid line corresponds to the approximation (42).

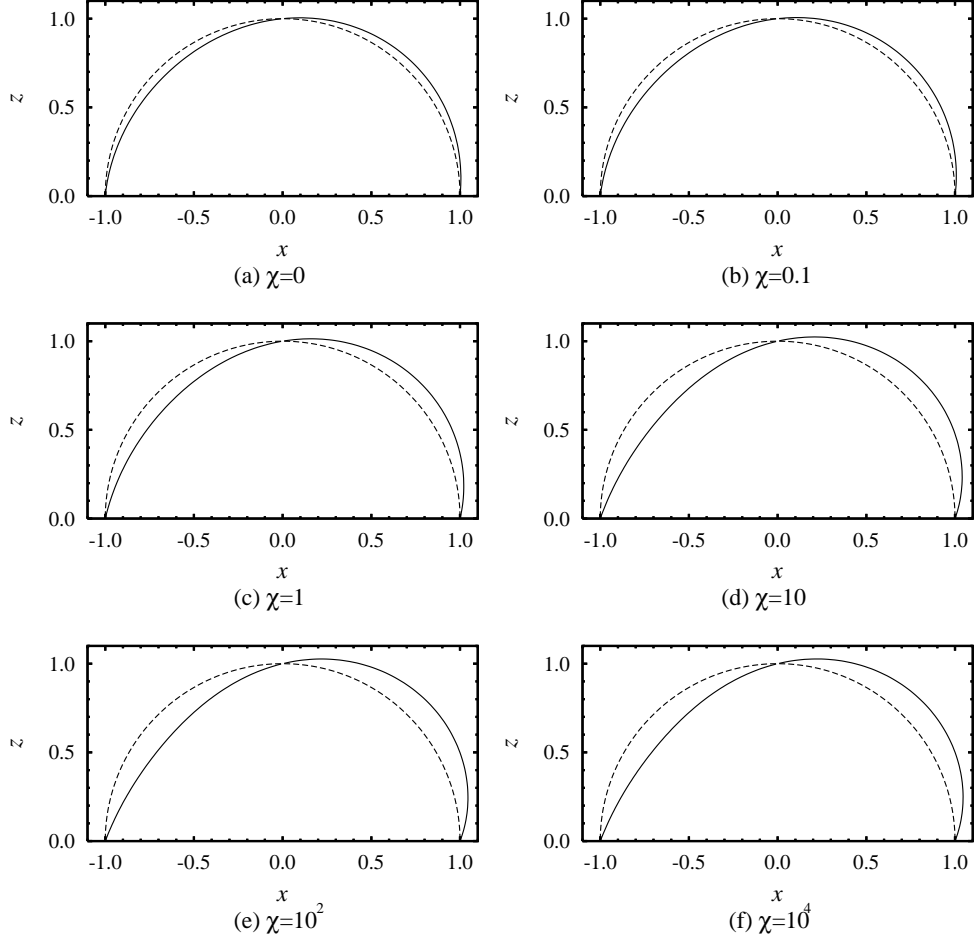


FIG. 5: Shape of the bump on the plane of $y = 0$ for various viscosity ratios χ . The dashed line shows the hemisphere with no deformation. The solid line shows the deformed interface for a Capillary number $Ca = 0.05$.

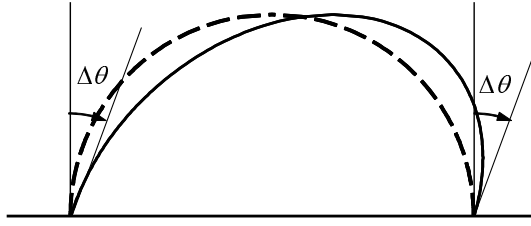


FIG. 6: Advancing and receding contact angles due to deformations are introduced in the problem in the small Capillary number regime.

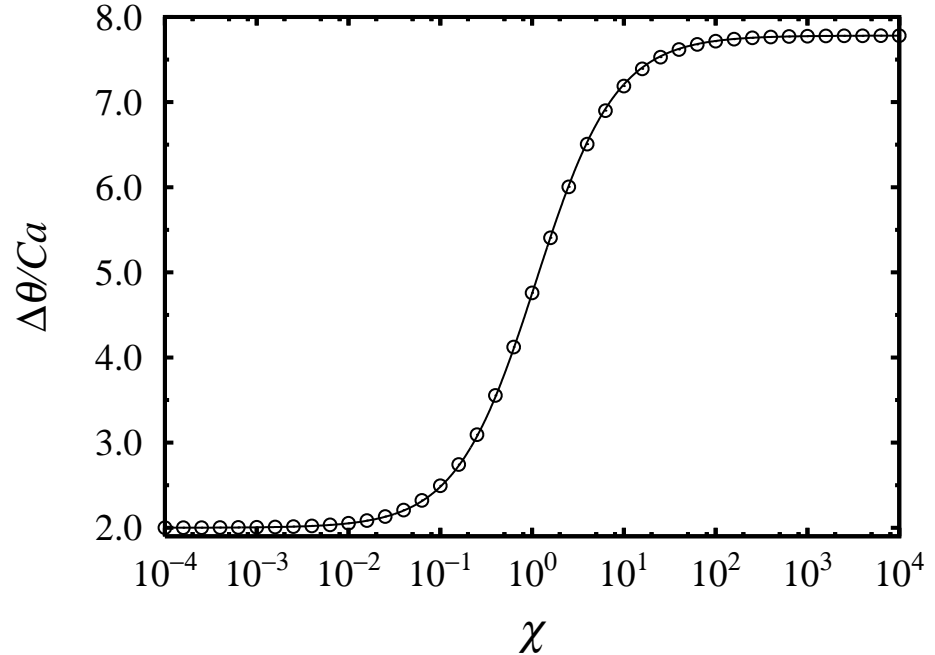


FIG. 7: Contact angle deformations as a function of the viscosity ratio in the limit of small Capillary numbers. The symbol \circ corresponds to the solution based on (50). The solid line corresponds to the approximation (58).

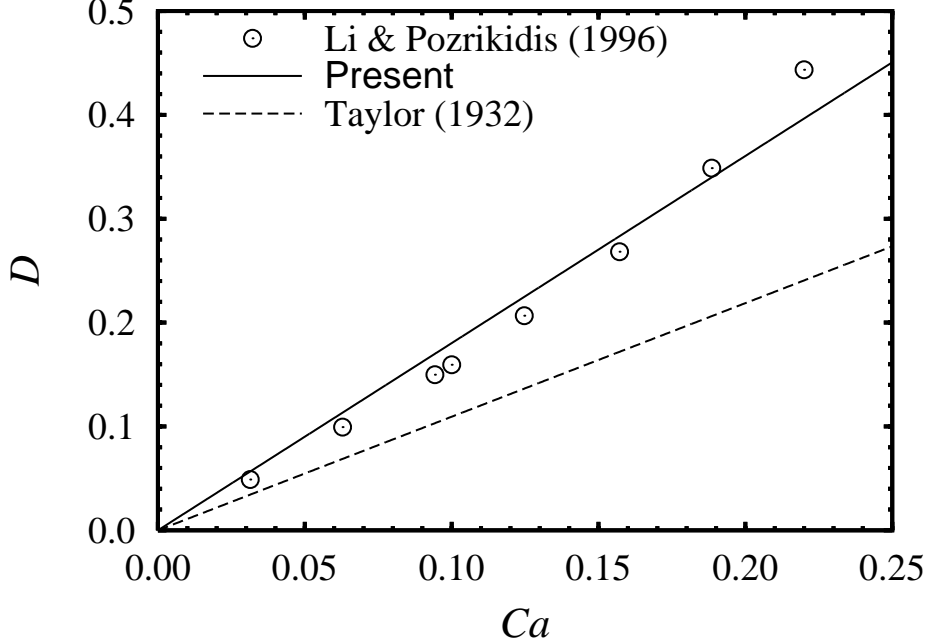


FIG. 8: Deformation parameter D as a function of the Capillary number for a viscosity ratio $\chi = 1$. Our solution (straight line) is compared with the results obtained with the boundary integral method (○) by Li and Pozrikidis (1996). The deformation parameter for the case of a droplet suspended in an infinite shear flow is also reported (dashed line).

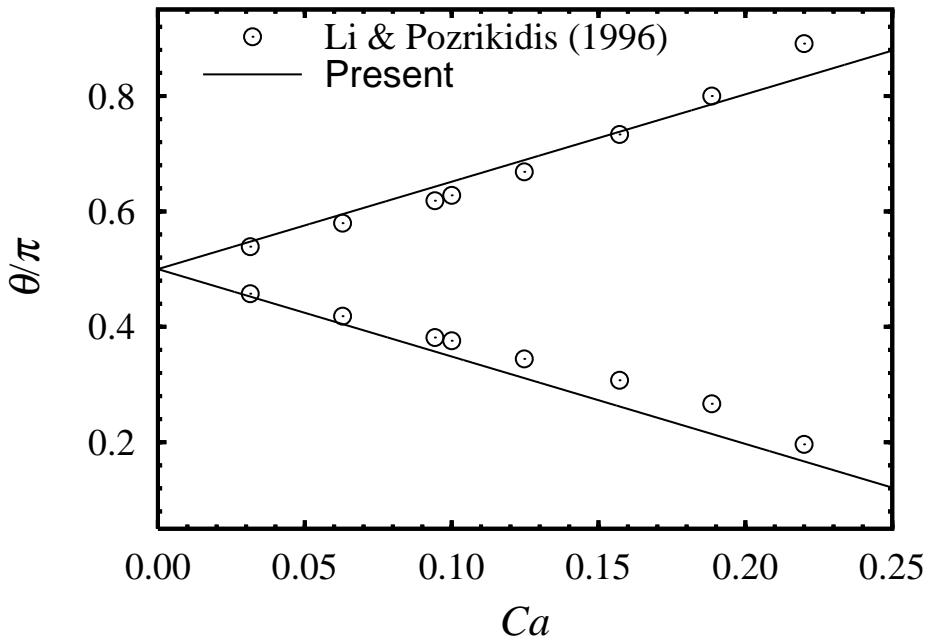


FIG. 9: Advancing and receding contact angles as a function of the Capillary number for a viscosity ratio $\chi = 1$. Our results (straight line) are compared with the numerical results obtained with the boundary integral method (○) by Li and Pozrikidis (1996).

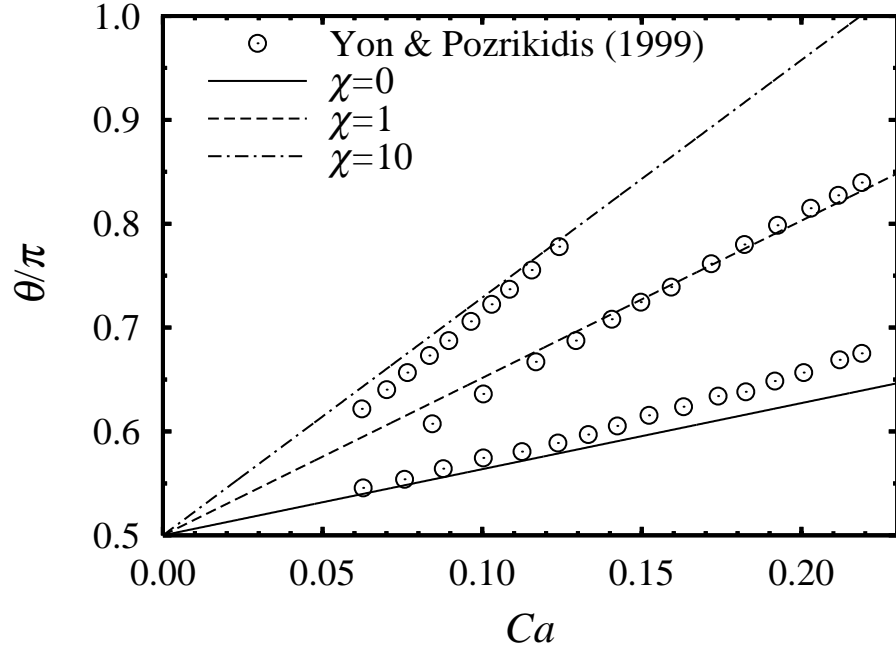


FIG. 10: Advancing contact angles as a function of the Capillary number for viscosity ratios $\chi = 0, 1, 10$. Our results are compared with the numerical results obtained with the boundary integral method (\circ) by Yon and Pozrikidis (1999).

[1] P.-G. de Gennes, F. Brochard-Wyart and D. Quere. *Capillarity and Wetting Phenomena: Drops, Bubbles, Pearls, Waves* (Springer, 2003).

[2] D.J. MacCann and R.G.H Prince. Regimes of bubbling at a submerged orifice. *Chem. Eng. Science* **26**, 1505 (1971).

[3] G. Duhar and C. Collin. A predictive model for the detachment of bubbles injected in a viscous shear flow with small inertial effects. *Phys. Fluids* **16**, L31-L34 (2004).

[4] J. Chatterjee. A criterion for Buoyancy induced drop detachment based on an analytical approximation of the drop shape. *Colloid Surf. A: Physicochem. Eng. Asp.* **178**, 249-263 (2001).

[5] M.E. O'Neill. A Sphere in contact with a plane wall in a slow linear shear flow. *Chem. Eng. Sc.* **23**, 1293-1298 (1968).

[6] W.A. Hyman. Shear flow over a protrusion from a plane wall. *J. Biomech.* **5**, 45-48; corrigendum on page 643 (1972).

[7] T.C. Price. Slow linear flow past a hemispherical bump in a plane wall. *Q. J. Mech. Appl. Math.* **38**, 93-104 (1985).

[8] C. Pozrikidis. Shear flow over a protuberance on a plane wall. *J. Eng. Math.* **31**, 29-42 (1997).

[9] V.E.B. Dussan and R. T.-P. Chow. On the ability of drops or bubbles to stick to non-horizontal surfaces of solids. *J. Fluid. Mech.* **137**, 1-29 (1983).

[10] V.E.B. Dussan. On the ability of drops or bubbles to stick to non-horizontal surfaces of solids. Part 2. Small drops or bubbles having contact angles of arbitrary size. *J. Fluid. Mech.* **151**, 1-20 (1985).

[11] V.E.B. Dussan. On the ability of drops or bubbles to stick to surface of solids. Part 3. The influence of the motion of the surrounding fluid on dislodging drops. *J. Fluid. Mech.* **174**, 381-397 (1987).

[12] P. Dimitrakopoulos and J. J. L. Higdon. Displacement of fluid droplets from solid surfaces in low-Reynolds number shear flows. *J. Fluid. Mech.* **336**, 351-378 (1997).

[13] P. Dimitrakopoulos and J. J. L. Higdon. On the displacement of three dimensional fluid droplets from solid surfaces in Low-Reynolds number shear flows. *J. Fluid. Mech.* **377**, 189-222 (1998).

[14] S. Yon and C. Pozrikidis. Deformation of a liquid drop adhering to a plane wall: significance of the drop viscosity and the effect of an insoluble surfactant. *Phys. Fluids* **11**, 1297-1308 (1999).

[15] X. Li and C. Pozrikidis. Shear flow over a liquid drop adhering to a solid surface. *J. Fluid. Mech.* **307**, 167-190 (1996).

[16] A.D. Schleizer and R.T. Bonnecaze. Displacement of a two-dimensional immiscible droplet adhering to a wall in shear and pressure-driven flows. *J. Fluid Mech.* **383**, 29-54 (1999).

[17] P. D. M. Spelt. Shear flow past two-dimensional droplets pinned or moving on an adhering channel wall at moderate Reynolds numbers: a numerical study. *J. Fluid Mech.* **561**, 439-463 (2006).

[18] K. Sarkar and A. Prosperetti. Effective Boundary conditions for Stokes flow over a rough surface. *J. Fluid Mech.* **316**, 223-240 (1996).

[19] M. Sbragaglia and A. Prosperetti. Effective velocity boundary condition at a mixed slip surface. *J. Fluid Mech.* in press (2006). See physics/0607003.

[20] E. Lauga and H. A. Stone. Effective slip in pressure-driven Stokes flow. *J. Fluid. Mech.* **489**, 55-77 (2003).

[21] W. Jager and A. Mikelic. On the roughness-induced effective boundary conditions for an incompressible viscous flow. *Jour. Diff. equations* **170**, 96-122 (2001).

[22] E. Lauga, M. Brenner and H. Stone. *Microfluidics: The no-slip boundary condition. Handbook of Experimental fluid dynamics*, Chapter 15 (Springer, 2005).

[23] C. Cottin-Bizonne, J.-L. Barrat, L. Bocquet and E. Charlaix. Low friction flows of liquids at nanopatterned interfaces. *Nature Mater.* **2**, 237 (2003).

[24] R. Benzi, L. Biferale, M. Sbragaglia, S. Succi and F. Toschi. Mesoscopic modelling of heterogeneous boundary conditions for microchannel flows. *J. Fluid. Mech.* **548**, 257-280 (2006).

[25] M. Sbragaglia, R. Benzi, L. Biferale, S. Succi and F. Toschi. Surface Roughness-Hydrophobicity Coupling in Microchannel and Nanochannel Flows. *Phys. Rev. lett.* **97**, 204503 (2006).

[26] P. Joseph, C. Cottin-Bizonne, J.-M. Benot, C. Ybert, C. Journet, P. Tabeling, and L. Bocquet. Slippage of Water Past Superhydrophobic Carbon Nanotube Forests in Microchannels. *Phys. Rev. Lett.* **97**, 156104 (2006).

[27] J. Ou, B. Perot and J. Rothstein. Laminar drag reduction in microchannels using ultrahydrophobic surfaces. *Phys. Fluids* **16**, 4635-4643 (2004).

[28] M. Sbragaglia and K. Sugiyama. Boundary induced non-linearities at small Reynolds numbers. *Physica D* submitted (2006). See cond-mat/0603500.

[29] C.-H. Chan and L. G. Leal. The motion of a deformable drop in a second-order fluid. *J. Fluid Mech.* **92**, 131-170 (1979).

[30] J. Magnaudet, S. Takagi and D. Legendre. Drag, deformation and lateral migration of a buoyant drop moving near a wall. *J. Fluid Mech.* **476**, 115-157 (2003).

[31] G.I. Taylor. The viscosity of a fluid containing small drops of another fluid. *Proc. R. Soc. Lond. A* **138**, 41-48 (1932).